SDC-92-210

# SDC
# SOLENOIDAL DETECTOR NOTES

## TRACKING SIMULATION STUDIES OF HIGGS BOSON DECAY TO FOUR LEPTONS

May 20, 1992

K. O'Shaughnessy
*University of California*

SCIPP 92/09
SDC 92-210
May 20, 1992

# Tracking Simulation Studies of Higgs Boson Decay to Four Leptons*

K. O'SHAUGHNESSY

*Santa Cruz Institute for Particle Physics*
*University of California, Santa Cruz, CA 95064*

* Work supported in part by the U.S. Department of Energy.

## INTRODUCTION

The process of Higgs boson production at SSC energies and the subsequent decay to four leptons (lepton is $e$ or $\mu$ in this case) is one of the most widely studied. Referred to as the "gold-plated" method of discovering the Higgs boson if its mass lies in the range 100-600 GeV/$c^2$, it has a very clear signature.[1] However, event rates are low (especially for high masses) and so the criteria for most SSC detector proposals have included the requirement of high efficiency for detecting high $p_t$ leptons as well as momentum resolution on the order of $\sigma_{p_t}/p_t = 0.25p_t$ (TeV$^{-1}$) and electromagnetic calorimeter resolutions on the order of $\sigma_E/E = .15/\sqrt{E}\oplus 0.01$.

Now that the SDC tracking system has been defined, it is possible to do more than a parametric estimate of the tracking resolutions and efficiencies. This note describes the simulation and reconstruction programs and resulting evaluation of performance of the SDC detector as was summarized in the chapter on the tracker in the Technical Proposal[2]. Two different masses were studied as well as the effect of increased luminosity. In addition, several variations of the baseline geometry were used to evaluate design options.

The following sections describe the event sample and the baseline configuration of the tracking detector. Effects included in the simulation are detailed and then the track reconstruction algorithm is discussed. Finally, an outline of the Higgs analysis procedure is given along with the results.

## EVENT SAMPLE

The decay of a neutral Higgs boson $H^0 \rightarrow Z^0 Z^0 \rightarrow 4\ell$ has been studied. For $m_H$=140 GeV/$c^2$, the decay modes were forced to be $e^+e^-e^+e^-$ (low mass $4e$) or $\mu^+\mu^-\mu^+\mu^-$ (low mass $4\mu$) and only design luminosity was run. The decay mode $e^+e^-\mu^+\mu^-$ was generated for $m_H$=300 GeV/$c^2$ at 1, 3 and 6 times design luminosity. The ISAJET generator was used to produce the Higgs event and PYTHIA minimum bias events were added as background. The design luminosity was simulated by a Poisson-distributed mean of 1.6 background events for each

bunch crossing, with a total of 7 crossings ($-4$ to $+2$ from the crossing with the Higgs) used to account for loopers and allow for drift times in the straw system. Only events where all four final state leptons had $|\eta| \leq 2.5$ were kept for further analysis. For the low mass case, it was also required that at least 2 of the leptons had $p_t$ of 40 GeV.

## Detector Geometry and Simulation

The geometry and simulation of the silicon tracker has been described in another note[3]. For completeness, a brief summary as well as a description of the straw system simulation will be given here.

The baseline detector for this study included an 8 layer barrel / 13 layer forward silicon tracker and a 5 layer straw outer tracker. Table 1 gives the positions and extent of the silicon tracker, Figure 1 is a side view of a quarter of the detector. Table 2 gives the values for the straw tracker used. Note that the straw system presented in the TDR was somewhat different; however, the performance differences are not relevant for this study. The simulation for the intermediate tracking detector (ITD) was not available and no attempt was made to use pixel detectors. Two variations of the silicon tracker were also used at one point in this study; the first was to keep the same geometry but ignore the information in the first two layers. The second was a redesigned layout with 6 layers in the barrel and 11 layers in each forward section (see Table 3).

The interaction of the particles with the detector is GEANT based. Therefore processes such as photon conversion, bremsstrahlung and hadronic interactions are included. Also, the simulation generated out-of-time crossings and accounted for hits that occured within the active time windows for the systems. For the silicon tracker, the smallest units described as GEANT volumes are individual silicon wafers. In the barrel region, the double-sided wafers have 50 $\mu$m pitch, 10 mr stereo strips on the ohmic side and are 6 cm long. There is a dead area of 600 $\mu$m defined on the sides and ends of the wafers. Two wafers are assumed to be bonded

**Table 1.**

Dimensions for baseline silicon tracker

| Barrel | r | z extent | | Silicon Area |
|---|---|---|---|---|
| (1) | 9 cm | 30 cm | | |
| (2) | 12 cm | 30 cm | | |
| (3) | 18 cm | 30 cm | | 6.78 $m^2$ for Barrel |
| (4) | 21 cm | 30 cm | | |
| (5) | 24 cm | 30 cm | | |
| (6) | 27 cm | 30 cm | | |
| (7) | 33 cm | 30 cm | | |
| (8) | 36 cm | 30 cm | | |
| **Disks** | $r_{in}$ | $r_{out}$ | z | **Silicon Area** |
| (1) | 15 cm | 39 cm | 33 cm | |
| (2) | 15 cm | 39 cm | 38 cm | |
| (3) | 15 cm | 39 cm | 44 cm | 10.16 $m^2$ for Disks |
| (4) | 15 cm | 39 cm | 52 cm | (both sides) |
| (5) | 15 cm | 39 cm | 61 cm | |
| (6) | 15 cm | 39 cm | 72 cm | |
| (7) | 15 cm | 39 cm | 85 cm | |
| (8) | 15 cm | 39 cm | 102 cm | |
| (9) | 15 cm | 39 cm | 122 cm | |
| (10) | 22.5 cm | 46.5 cm | 146 cm | |
| (11) | 28.5 cm | 46.5 cm | 182 cm | |
| (12) | 34.5 cm | 46.5 cm | 218 cm | |
| (13) | 40.5 cm | 46.5 cm | 258 cm | |
| | | Total Area = 16.94 $m^2$ | | |

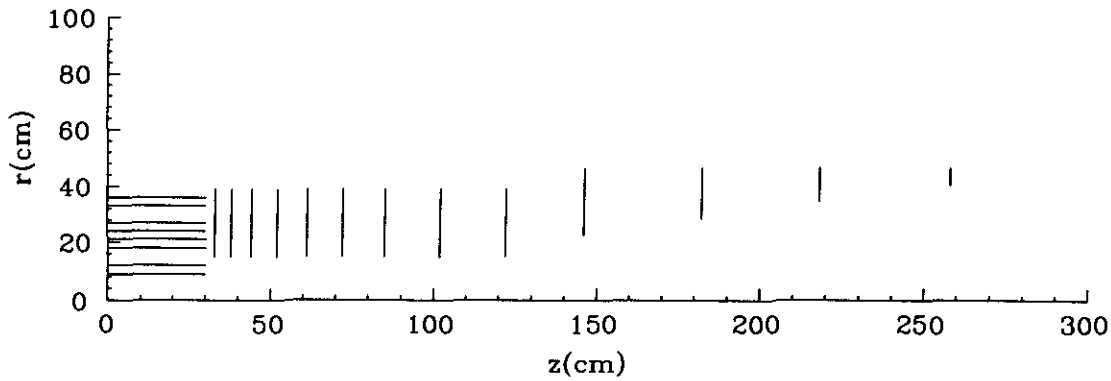


Figure 1. Silicon tracker design.

**Table 2**

Barrel Outer Tracking System Configuration

| Superlayer | Mean Radius (m) | Layers/ Superlayer | $z_{max}$ (m) | Stereo Angle (°) |
|---|---|---|---|---|
| 1 | 0.718 | 6 | 2.80 | 0 |
| 2 | 1.051 | 6 | 3.20 | +3 |
| 3 | 1.360 | 8 (trigger) | 3.90 | 0 |
| 4 | 1.489 | 6 | 3.95 | −3 |
| 5 | 1.625 | 8 (trigger) | 3.95 | 0 |

together to form a 12 cm long readout unit. The readout units are tilted at an angle of 7.5 degrees to account for the Lorentz angle (see Figure 2).

In the forward region, the 6 cm long wafers are wedge-shaped, again have 10 mr stereo angle on the ohmic side and are bonded together to form the readout units. The pitch is 50 $\mu$m at the location of the readout chips, which is usually placed close to the outer edge of the readout unit. Thus the pitch typically ranges from 28 to 51 $\mu$m over the radial extent of the unit. Figure 3 shows how these readout units are placed around the cooling ring to make up one of the forward layers; the readout units alternate $\pm 1$ cm in $z$ around the nominal position as $\phi$

**Table 3.**

Dimensions for reduced silicon tracker

| Barrel | r | z extent | | Silicon Area |
|---|---|---|---|---|
| (1) | 9 cm | 30 cm | | |
| (2) | 12 cm | 30 cm | | 5.09 $m^2$ for Barrel |
| (3) | 21 cm | 30 cm | | |
| (4) | 24 cm | 30 cm | | |
| (5) | 33 cm | 30 cm | | |
| (6) | 36 cm | 30 cm | | |
| **Disks** | $r_{in}$ | $r_{out}$ | z | **Silicon Area** |
| (1) | 15 cm | 39 cm | 33 cm | |
| (2) | 15 cm | 39 cm | 41 cm | |
| (3) | 15 cm | 39 cm | 50 cm | 9.00 $m^2$ for Disks |
| (4) | 15 cm | 39 cm | 62 cm | (both sides) |
| (5) | 15 cm | 39 cm | 75 cm | |
| (6) | 15 cm | 39 cm | 90 cm | |
| (7) | 15 cm | 39 cm | 110 cm | |
| (8) | 22.5 cm | 46.5 cm | 136 cm | |
| (9) | 22.5 cm | 46.5 cm | 168 cm | |
| (10) | 34.5 cm | 46.5 cm | 208 cm | |
| (11) | 34.5 cm | 46.5 cm | 255 cm | |
| | | Total Area = 14.09 $m^2$ | | |

increases to decrease the effects of dead space and to allow for cable runs.

The straw system uses cylinders as the basic active media for each straw layer. These cylinders have a radius equal to the nominal radius of a layer of straws and a depth equal to $\sqrt{3}$ times the width of a straw. Although this is not the same as the designed trapezoidal close-packed modules, it is a compromise to allow faster simulations. The conversion from a hit in this cylinder to a time measured on a wire is described below.

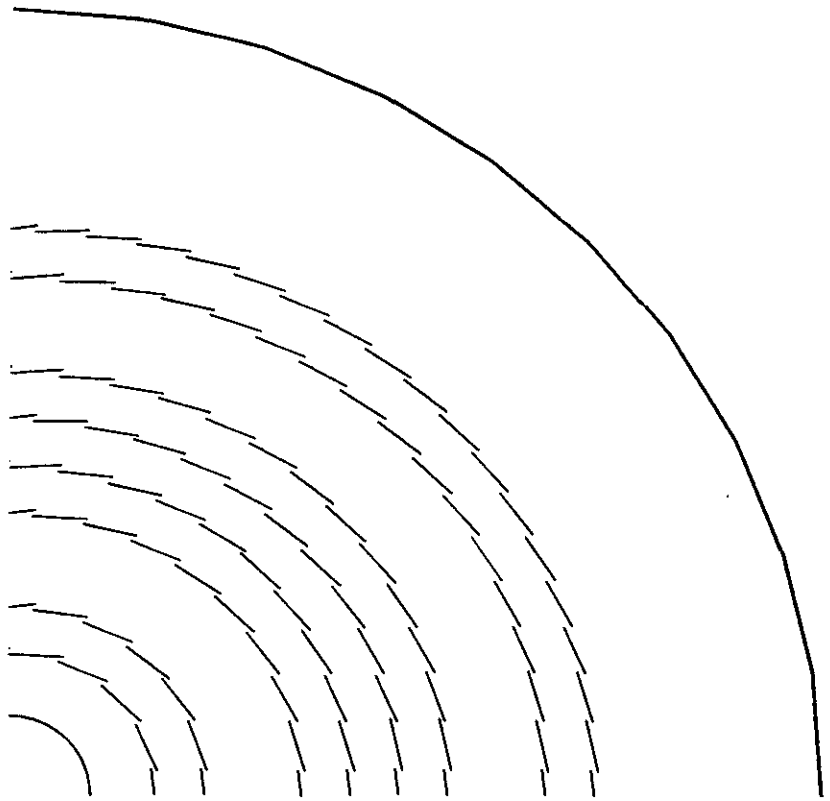

Figure 2. End view of the barrel showing the tilted wafers.
The solid curves show the gas enclosure volume.

The other aspect of the geometry description which effects this analysis is that of support and dead material. In addition to the active material described above, each system has attempted to approximate the extra material. Table 4 summarizes this material and gives the number of radiation lengths at normal incidence. The innermost material is the beampipe which is at $r$=2.5 cm and is 0.038 cm thick. The silicon system is contained in a gas enclosure vessel with a 0.5 mm thick Be inner wall at $r$=5 cm and a 1 mm thick Be wall at $r$=50 cm. The support and cooling ring structures have been approximated by a cylinder at the nominal radius of the layer and with a given number of radiation lengths. The inner two layers have had this support adjusted to reflect the fact that the first suppport ring occurs between layers 2 and 3. A more complete study of the material in the silicon system was performed[4] and the numbers used were adjusted to reflect the findings.

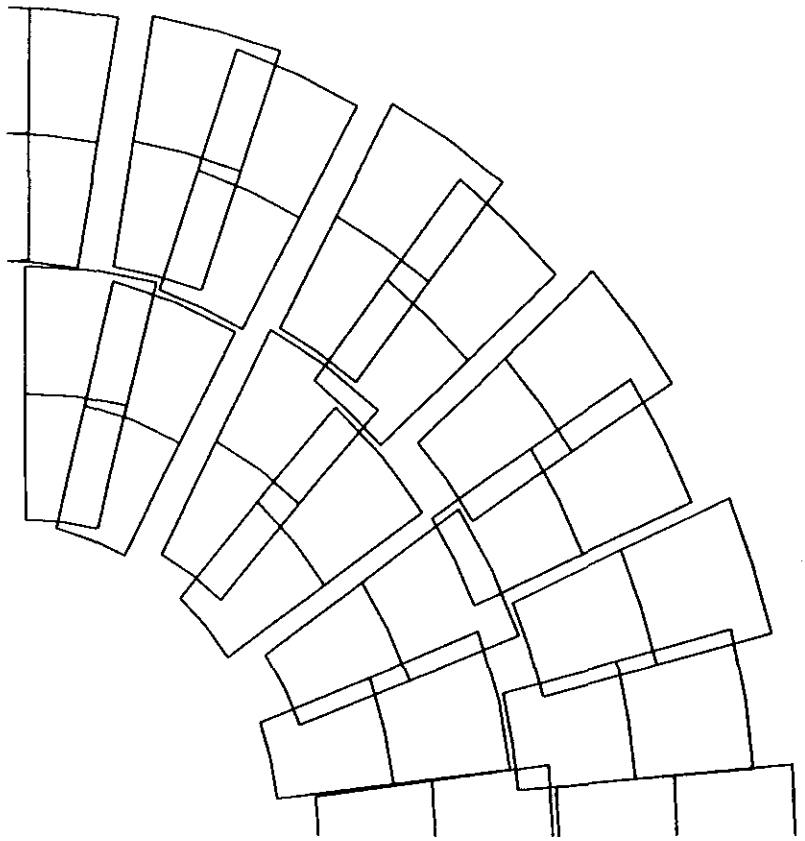

Figure 3. Angled view of a section of the forward wafers.

The dead material entered in the straw simulation consists of two carbon fiber support cyliners at the inner radius of each superlayer. The simulation version used for this study did not include any endplates or other support material.

A simple model of the deposition of energy in the silicon wafers was used to convert the GEANT energy loss into strips hit. No attempt was made to include the effects of the magnetic field or of charge diffusion; the energy was assigned to the strips crossed by the particle. After all particles have been processed, a strip was considered 'hit' if the energy for a given strip was greater than a threshold

**Table 4**

Dead material in the tracker simulation at $\eta$=0.

| Inner radius(cm) | Thickness (cm) | Material | $X_0$ (%) | Description |
|---|---|---|---|---|
| 2.5 | 0.038 | Be | 0.11 | beampipe |
| 5.0 | 0.050 | Be | 0.14 | gas inner liner |
| 8.5 | 1.0 | diffuse Si | 0.20 | support for layer 1 |
| 11.5 | 1.0 | diffuse Si | 0.20 | support for layer 2 |
| 17.5 | 1.0 | diffuse Si | 0.50 | support for layer 3 |
| 20.5 | 1.0 | diffuse Si | 0.35 | support for layer 4 |
| 23.5 | 1.0 | diffuse Si | 0.35 | support for layer 5 |
| 26.5 | 1.0 | diffuse Si | 0.35 | support for layer 6 |
| 32.5 | 1.0 | diffuse Si | 0.35 | support for layer 7 |
| 35.5 | 1.0 | diffuse Si | 0.35 | support for layer 8 |
| 50.0 | 0.1 | Be | 0.28 | gas outer liner |
| Radiation Lengths for Silicon system support = 0.0318 $X_0$ | | | | |
| 69.7 | 0.0254 | C | 0.14 | cylinder 1a |
| 70.7 | 0.0254 | C | 0.14 | cylinder 1b |
| 102.0 | 0.0254 | C | 0.14 | cylinder 2a |
| 103.0 | 0.0254 | C | 0.14 | cylinder 2b |
| 132.7 | 0.0254 | C | 0.14 | cylinder 3a |
| 133.7 | 0.0254 | C | 0.14 | cylinder 3b |
| 145.9 | 0.0254 | C | 0.14 | cylinder 4a |
| 146.9 | 0.0254 | C | 0.14 | cylinder 4b |
| 159.1 | 0.0254 | C | 0.14 | cylinder 5a |
| 160.1 | 0.0254 | C | 0.14 | cylinder 5b |
| Radiation Lengths for Straw system support = 0.0140 $X_0$ | | | | |
| Total Radiation Lengths in Tracking system = 0.102 $X_0$ | | | | |

(set to approximately 1/3 mip). At this point, the effects of noise, inefficiencies and dead time are not included.

As the tracks pass through the straw cylinders, the interaction position is converted to a wire and a time. After all tracks have been processed, the times are adjusted by the drift and propogation times and required to be within a window of approximately $\pm 50$ ns. Also, hits that occur within 40 ns of another hit are deleted. The options of adding noise and inefficiencies were not used.

## Track Reconstruction and Fitting

The reconstruction program used to find the tracks is based on clustering segments determined from the silicon system. The method has been described in Reference 5 but will be summarized here.

Both coordinates (reconstructed 3 dimensional space points) and segments (local track vectors) are reconstructed from the hit information of the silicon strips. For the barrel, the axial and stereo strips on the wafer are associated simply by how close the strip numbers are; one stereo strip crosses 24 axial strips over the 12 cm length of the readout unit. The knowledge of the geometrical position of the wafers (assuming perfect alignment) then allows a determination of $r$, $\phi$ and $z$ of the hits as well as the errors on those quantities. If no stereo assignment is made to an axial hit, the the $z$ position is taken as the middle of the readout unit. The coordinates reconstructed in the forward layers are similar with the roles of $r$ and $z$ interchanged.

Segments are formed between two adjacent silicon layers to give an local track vector. All layers except the extreme inner and outer layers are used twice; *eg* segments are formed between layers 1 and 2 as well as 2 and 3. The coordinate in the inner layer is matched to the nearest coordinate in $\phi$ in the next layer within some window set by a $p_t$ cut (typically 0.75 GeV). If there is more than one option, then up to 3 segments are formed. The quantities calculated for each segment assume that the track comes from the origin and are the curvature $\rho$ ($=.3\mathrm{B}/p_t$), $\phi_0$, $z_0$ and

$\tan\lambda$ ($\lambda$ is the dip angle); all are calculated at the distance of closest approach to the origin.

The above set of parameters leads to a conceptually elegant track finding method. If one considers a 2-D space of the bending plane variables $\rho$ and $\phi_0$ and plots the segments found and their errors, the segments from the same track should cluster together. A $\chi^2$ association can be made that follows this visual method. Allowance for multiple scattering can be made by adding a term to the errors; some arbitration can be made if tracks within jets, for example, end up in the same cluster. The end result is a set of points (the ones that made up the segments) and an initial guess at the track parameters to use in a fit procedure.

The next step in the track reconstruction is to do a 5 parameter iterative fit. In addition to the parameters listed above, the impact parameter $b_0$ is added. The fit includes an estimate of the multiple scattering in the silicon layers. Some passes are also made which delete points that contribute substantially to the $\chi^2$ of the track and pick up points that were missed.

The reconstruction program then uses these tracks to extrapolate to the outer system to pick up information there. The straw system first reconstructs local segments within the superlayers. The algorithm starts at the outer layer of each superlayer and starts seed tracks within a road, looking in. It then skips to the inner layer and works outward. The drift times are fit with each addition of a hit and the end result is a $\phi$ position, curvature, resolution of right-left ambiguity (if possible) and $t_0$ for a list of segments in each straw superlayer. The silicon track is extrapolated to the first superlayer and a search is made to see if a segment matches both the $\phi$ position and the estimated curvature. The segment is treated as a single point added to the track, the track is refit and the road continues outward. (This same road technique can be used to add information from the ITD and optional pixel layers, but wasn't done in this case.)

## HIGGS ANALYSIS PROCEDURE

The goals of the analyses at the two masses were slightly different, but the procedures were very similar. For the 300 GeV case, determining and optimizing the efficiency for reconstructing the Higgs was the primary goal, with understanding the difference between the electron and muon modes an additional result. No attempt was made to detemine mass resolutions. For the low mass 4e and $4\mu$ samples, the main result was the resolution for the Higgs mass.

In both cases, the analysis started with the tracks found using the method described in the previous section. It was assumed that information from the muon system or calorimeter would give an identification of electron or muon; so the Monte Carlo identity was used to select tracks as lepton candidates. Muons were then required to have a reconstructed $p_t$ greater than 10 GeV/$c$. Several options were available for electrons, depending on whether the goal was efficiency for passing an E/p cut or better resolution. Due to bremsstrahlung in the tracker, it is expected that a momentum determined from the silicon tracker alone would better match the true momentum. However, due to the shorter track length, the resolution would be worse. This effect can be seen in Figure 4a which shows the ratio of the generated momentum $p_{gen}$ over the fit momentum $p_{fit}$ for electrons using silicon alone (open) and silicon and straws (hatched). What is not shown in the plot is the fact that the silicon alone had 24 tracks that overflowed the histogram while the silicon and straw fit had only 8. Figure 4b shows the momentum resolution for single electrons at varying $p_t$ values for silicon alone and silicon and straws. A 10 GeV $p_t$ cut was also made on the electron candidates after the optional refit with silicon alone, then the $p_{gen}/p_{fit}$ cut was made. For this note, the acceptable range of $p_{gen}/p_{fit}$ values was always $0.7 < p_{gen}/p_{fit} < 1.4$.

Once the list of acceptable leptons had been produced, the next stage was to match up the pairs corresponding to $Z^0$'s (real or virtual). Pairs of opposite sign, same type leptons were made and their invariant mass calculated. The list of pairs was ordered according to closeness of the invariant mass to 91 GeV/$c^2$. The list

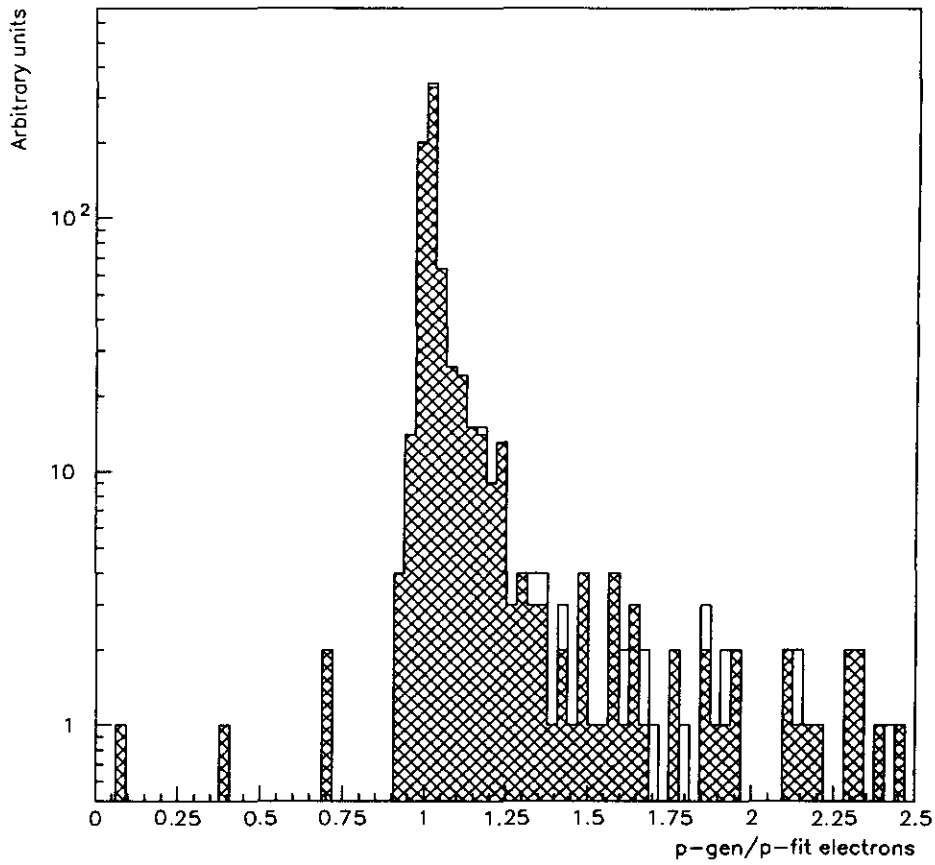


Figure 4a. Comparison of $p_{gen}/p_{fit}$ distributions for fitting with silicon alone (hatched) and with silicon and straws (open).

was reduced by allowing each lepton to appear only once. It was then possible to make cuts on the $Z^0$ candidates to be within a $\pm 10$ GeV window around the $Z^0$ mass (on only one candidate for the low mass Higgs case). Although the pairing of leptons for the $e^+e^-\mu^+\mu^-$ mode was mostly straightforward, in some events high $p_t$ leptons from $b$ decays or conversions were present which had the potential of creating a combinatoric background. For events with 2 $Z^0$ candidates the last step was to calculate the 4 lepton invariant mass.

The efficiency results for the $m_H$=300 GeV/$c^2$ decay to $e^+e^-\mu^+\mu^-$ are shown in Table 5 for the different luminosities. The single track efficiency was calculated for all tracks with $p_t > 10$ GeV. A MC track was defined as "findable" if it was not a strange baryon, was produced with $b_0 < 0.1$ cm, $|z_0| < 15$ cm and had

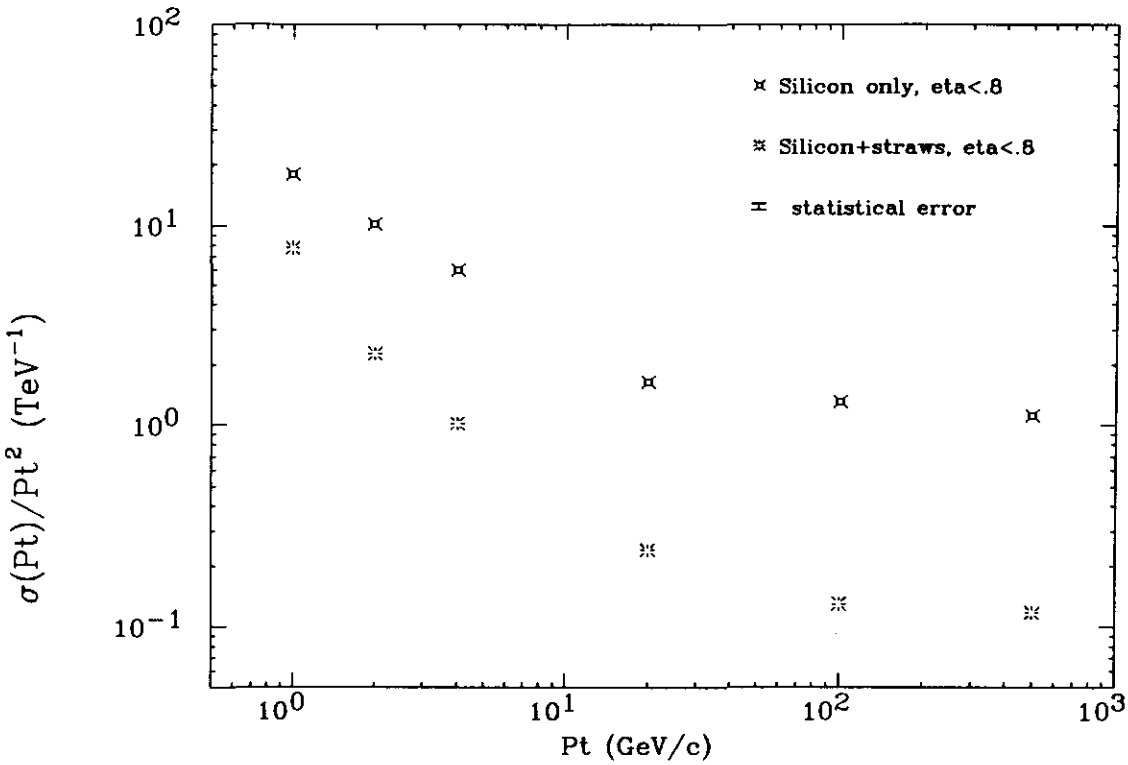


Figure 4b. Transverse Momentum resolution with silicon alone and silicon plus straws.

**Table 5**

Summary of efficiencies for $H^0 \rightarrow e^+e^-\mu^+\mu^-$ events ($m_H$=300 GeV/$c^2$) for various configurations.

| Luminosity | Layers barrel | Layers forward | Track efficiency $p_t$>10 GeV/$c$ | Electron $E/p$ efficiency 0.7<E/p<1.4 | $M_Z$ cut efficiency $e$ | $M_Z$ cut efficiency $\mu$ | Higgs reconstruction efficiency |
|---|---|---|---|---|---|---|---|
| $1 \times 10^{33}$ | 8 | 13 | 0.991 | $0.96 \pm 0.01$ | $0.99 \pm 0.01$ | $0.99 \pm 0.01$ | $0.84 \pm 0.04$ |
| $3 \times 10^{33}$ | 8 | 13 | 0.989 | $0.96 \pm 0.01$ | $1.00 \pm 0.01$ | $0.97 \pm 0.01$ | $0.83 \pm 0.04$ |
| $6 \times 10^{33}$ | 8 | 13 | 0.972 | $0.93 \pm 0.01$ | $1.00 \pm 0.01$ | $0.93 \pm 0.02$ | $0.75 \pm 0.04$ |
| $1 \times 10^{33}$ | 6(ignore 2) | 13 | 0.963 | $0.93 \pm 0.01$ | $0.99 \pm 0.01$ | $0.97 \pm 0.01$ | $0.71 \pm 0.04$ |
| $6 \times 10^{33}$ | 6(ignore 2) | 13 | 0.956 | $0.93 \pm 0.01$ | $1.00 \pm 0.01$ | $0.90 \pm 0.01$ | $0.65 \pm 0.04$ |
| $1 \times 10^{33}$ | 6 | 11 | 0.949 | $0.94 \pm 0.01$ | $0.98 \pm 0.01$ | $0.99 \pm 0.01$ | $0.72 \pm 0.03$ |

$p_t$ >1 GeV/$c$ and $|\eta| < 2.5$. The track was defined as "found" if it had at least 8 hits (axial or stereo) or 6 hits and 1 straw segment and if its hits matched up with a MC track with no more than 2 of its hits from another track. The efficiency for detecting the electrons and muons was slightly higher than for all tracks. For leptons with $p_t > 12.5$ GeV/$c$, the efficiencies for electrons (muons) in the baseline detector were: 0.992 (0.990) at $1\times10^{33}$, 0.984 (0.989) at $3\times10^{33}$, and 0.975 (0.986) at $6 \times 10^{33}$.

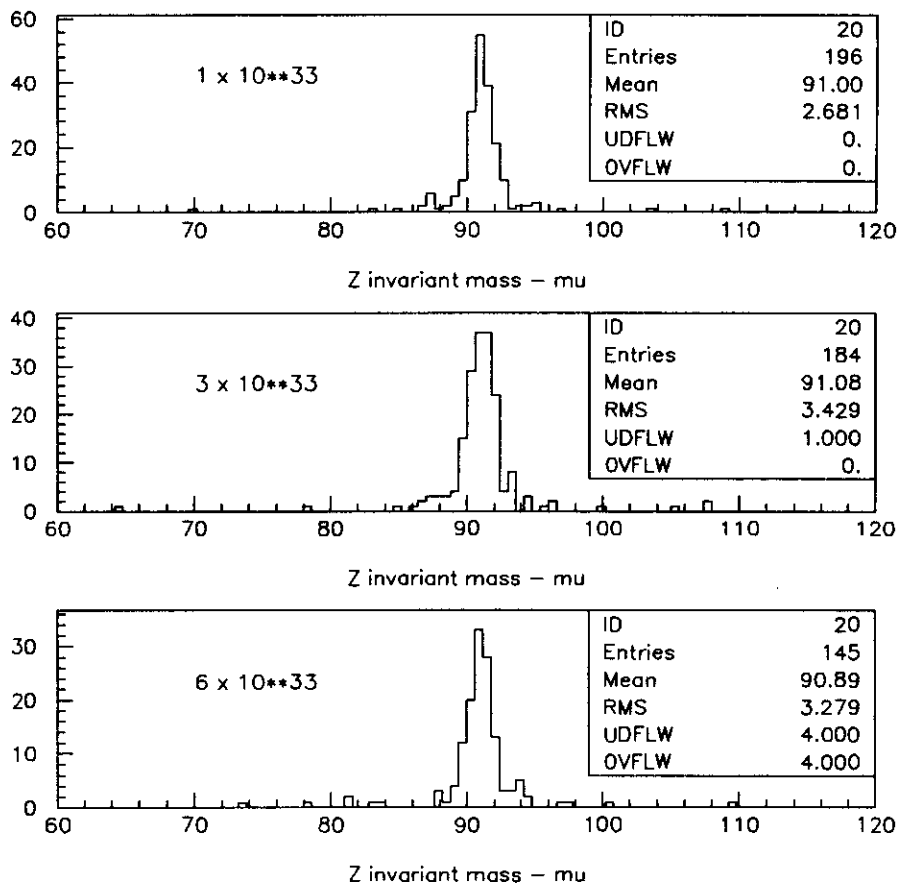


Figure 5. $Z^0$ invariant mass calculated from mu pairs as a function of luminosity.

For this mass, electrons were refit using only the silicon information before the $p_t$ cut and $p_{gen}/p_{fit}$ cut. After that point, the smeared generated momenta were used for the invariant mass calculations, and it can be seen that the efficiency for

the $Z^0$ formed from electrons to pass the invariant mass cut is correspondingly high. If the silicon and straw tracking system is used, the number is more typically 0.93. The $Z^0$ invariant mass as calculated from the muon pair is shown in Figure 5 for the 3 different luminosities. The final reconstructed efficiency for the Higgs (with no requirement on the reconstructed mass) is $0.84 \pm 0.04$(stat) and is quite stable under an increase in luminosity.

Also included in Table 5 are the results from the configurations 6a (ignore inner two barrel layers) and 6b (6 layer barrel/11 layer forward). The single track efficiency is worse than the baseline which is the main contribution to the drop in Higgs reconstruction efficiency.

At a Higgs mass of 140 GeV/$c^2$, the $p_t$ spectrum of the leptons is such that the expected four lepton invariant mass calculated using the reconstructed momentum should rival that calculated from the calorimeter. Therefore a study was done using the baseline detector at $1 \times 10^{33}\text{cm}^{-2}\text{s}^{-1}$ luminosity and the reconstruction algorithms outlined above to produce the four-lepton invariant mass. If no cut is made around the nominal Higgs mass, then the reconstruction efficiency was 65% for the $4e$ mode and 96% for the $4\mu$ mode. The difference between the two was a 91% efficiency for the $p_{gen}/p_{fit}$ cut for each of the four electrons (again, the lower efficiency compared to that listed in Table 5 is due to trying to get the better momentum measurement). The $4\mu$ efficiency is higher than in Table 5 because it doesn't include the two factors of $p_{gen}/p_{fit}$ efficiency and because only one $Z^0$ invariant mass cut is made.

The resolution results are shown in Figure 6a for the $4\mu$ mode and in Figure 6b for the $4e$ mode. The momentum used in both cases was that from the full silicon and straw system; the desire was to get the optimal resolution from the tracker. Fitting with a simple Gaussian function around the peak, the mass resolution was 1.0 GeV for the $4\mu$ mode and 2.3 GeV for the $4e$ mode. For comparison, a parameterized expectation is about 0.8 GeV[2]. Thus the bremsstrahlung and resulting errors in electron momentum reconstruction significantly effects the use

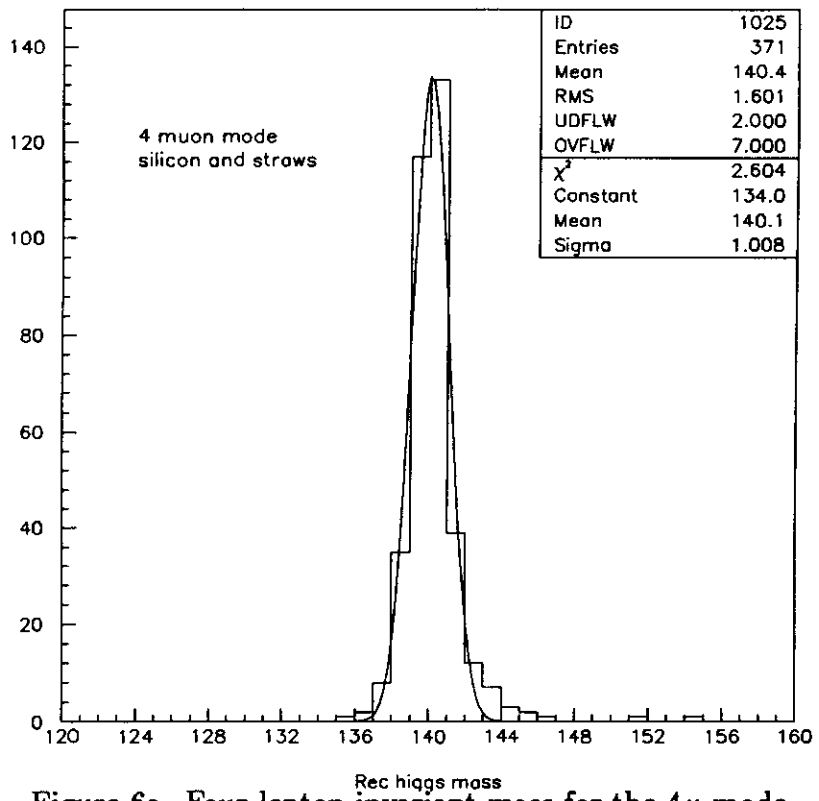


Figure 6a. Four lepton invariant mass for the $4\mu$ mode.

of the electron channel to reconstruct such low Higgs masses.

## SUMMARY

A study of tracking reconstruction effects on $H \rightarrow 4\ell$ decays was made for two Higgs boson masses and at several luminosities using essentially the baseline tracking system as described in the SDC Technical Design Report. The $p_t > 10$ GeV/$c$ single track finding efficiency was high and stable from $1-6 \times 10^{33}\text{cm}^{-2}\text{s}^{-1}$ luminosity. Bremsstrahlung effects on the electrons required some compromise between efficiency for an E/p-like cut and momentum resolution; further work on this issue could yield better results.

The reconstruction efficiency for Higgs bosons with masses of 300 GeV/$c^2$ was found to be 84% at design luminosity, using the $H \rightarrow e^+e^-\mu^+\mu^-$ channel. For a Higgs boson of mass 140 GeV/$c^2$, a rough measurement of the mass resolution

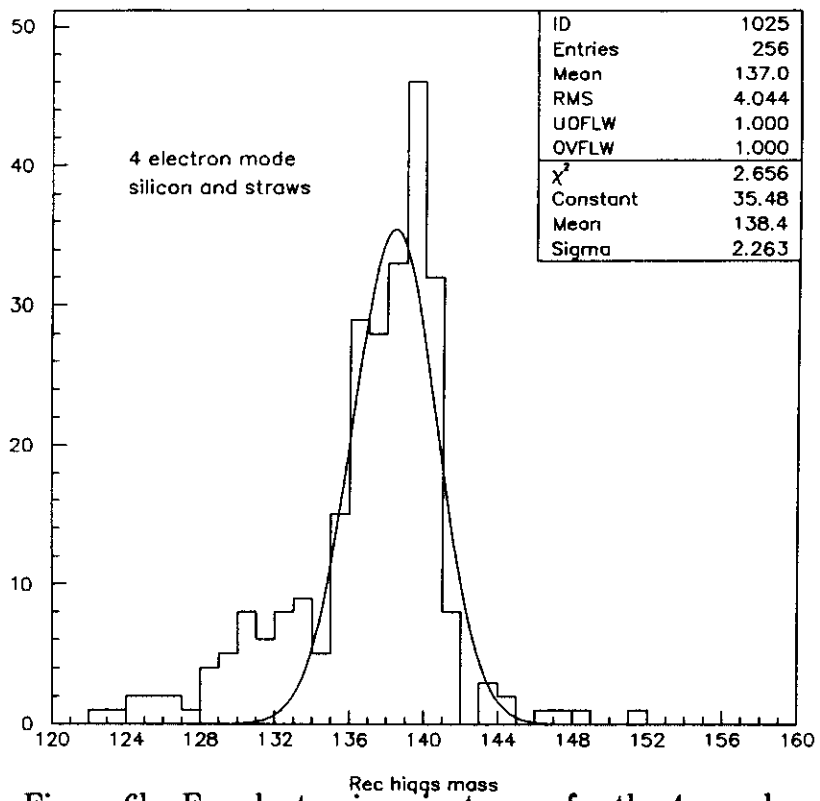


Figure 6b. Four lepton invariant mass for the $4e$ mode.

yielded $\sigma = 1.0$ GeV for $H \rightarrow 4\mu$ compared to a parameterized prediction of 0.8 GeV. The resolution was 2.3 GeV for $H \rightarrow 4e$, where again the effects of bremsstrahlung are felt.

## REFERENCES


[1] E.M. Wang *et al*, High Energy Physics in the 1990s, Snowmass 1988, S. Jensen, *ed.*, p. 109 and references therein.

[2] SDC Technical Design Report SDC-92-201.

[3] B.Hubbard *et al*, SDC-92-208.

[4] A. Palounek, SDC-92-255.

[5] B. Hubbard *et al*, SDC-92-209.